

First-principles calculation of the Coulomb interaction parameters U and J for actinide dioxidesJean-Baptiste Morée,^{1,*} Robinson Outerovitch,^{1,†} and Bernard Amadon^{1,2,‡}¹CEA, DAM, DIF, 91297 Arpajon Cedex, France²Université Paris-Saclay, CEA, Laboratoire Matière en Conditions Extrêmes, 91680 Bruyères le Châtel, France

(Received 21 January 2020; revised 30 July 2020; accepted 23 December 2020; published 11 January 2021)

We present *ab initio* calculations of effective interaction parameters U and J for dioxides of actinides from uranium to curium. We first use a self-consistent scheme using DFT + U and constrained random phase approximation (cRPA). For UO_2 , and NpO_2 , we find self-consistent values of U and J leading to values of gap in agreement with experiments. For PuO_2 , the value of U is underestimated. For AmO_2 and CmO_2 , we find very low self-consistent values. We compare projected local orbital Wannier functions to maximally localized Wannier functions and find a weak effect of the localization on interaction parameters. We suggest that spin-orbit coupling, and antiferromagnetism, could improve these results partially. We also extend our calculations by treating the p bands from oxygen as correlated, as in Seth *et al.* [Phys. Rev. Lett. **119**, 056401 (2017)], and show that the results are rather independent of self-consistency in this approach. Comparing these calculations, our conclusion is that including electron interaction on oxygen p orbitals is necessary both to improve the density of states and to compute more meaningful and predictive values of effective interaction parameters.

DOI: [10.1103/PhysRevB.103.045113](https://doi.org/10.1103/PhysRevB.103.045113)**I. INTRODUCTION**

Dioxides of actinides from U to Pu present an insulating behavior [1–3], in contrast to the corresponding actinide metals [4].¹ Qualitatively, $5f$ states separate in two Hubbard bands, whereas occupied $2p$ states from oxygen hybridize progressively with the lower Hubbard band when the atomic number of the considered actinide is increased. As a result, while UO_2 behaves as a Mott-Hubbard insulator [5,6], a crossover between Mott-Hubbard-type and charge-transfer-type insulating behavior is occurring around NpO_2 [5]. For these systems, density-functional theory (DFT) [7,8], associated with its traditional functionals such as local density approximation (LDA) [8] or generalized gradient approximation (GGA) [9], fails to reproduce correctly the spectral and structural properties—due to the poor description, within these schemes, of strong correlations between f electrons.

Several improvements to DFT have been used in order to describe these systems. Self-interaction corrections (SIC) [10], or hybrid functionals such as the Heyd-Scuserai-Ernzerhof (HSE) screened Coulomb hybrid functional [11], have improved the description of the electronic structure of early actinide dioxides [12–15]. Another possibility is to take into account explicitly the interaction between correlated electrons, as in the DFT + U [16], the combination of DFT with dynamical mean-field theory (DMFT) [17–19], and the Gutzwiller approximation [20]. These methods have improved the description of the electronic structure of early actinide dioxides as well [21–28]. However, in these frameworks and applications, values of direct and exchange parts of effective

interaction among correlated orbitals—denoted respectively U and J —remain most often input parameters. Within a theoretical framework, the *ab initio* determination of these parameters is desirable.²

The first step towards the *ab initio* determination of U and J —giving an expected range of values—is the systematic analysis made by Kotani *et al.* [5] of the experimental photoemission spectra by using the Anderson impurity model; according to the latter analysis, for dioxides of actinides from U to Cm, U is expected to vary between 4.0 and 7.0 eV and J between 0.54 and 0.82 eV.

Later, Yin *et al.* [23] computed the effective interaction by using a self-consistent GW method, and found values of U ranging from 5.1 to 6.2 eV. These calculations used a full screening approach, in contrast to studies using the constrained random-phase approximation (cRPA) method.

Later, first-principles calculations of U and J within the cRPA method [31,32] have been performed [33–35]: in the case of UO_2 , Amadon *et al.* [33,34] start from the values of Kotani [5], and perform a self-consistent calculation within DFT + U and cRPA yielding $U = 5.0$ eV and $J = 0.6$ eV. In this work, self-consistency was shown to be essential. An important remark is that, one major interest of self-consistency is the suppression of the dependency of the cRPA value of U on the starting electronic structure (at least at the DFT + U level), which strongly reinforces the *ab initio* character of the calculation of U .

In the case of UO_2 , PuO_2 , and CmO_2 , Seth *et al.* [35] include interactions between $5f$ and $2p$ electrons in the scheme,

*jean.baptiste.moree@gmail.com

†Robinson.outerovitch@cea.fr

‡bernard.amadon@cea.fr

¹ CmO_2 and AmO_2 gaps have not been measured.²We emphasize that, in any case, values of U for actinide dioxides are expected to be larger than those found for pure actinides [29,30] because at least uranium, neptunium, and plutonium dioxides are insulating, so that the screening should be smaller.

in order to compute intrashell interactions U^{ff} and U^{pp} and intershell interaction U^{fp} , then use a shell folding scheme yielding $U = 4.6$ eV for UO_2 , $U = 5.3$ eV for PuO_2 and $U = 5.9$ eV for CmO_2 , starting from a GGA band structure. In these calculations, pp and pf interactions are shown to be essential but self-consistency was not used.³

Important questions arising from these works are the following. (1) Does self-consistency enable to obtain realistic values of U^{ff} , for dioxides of actinides from UO_2 to CmO_2 ? (2) What are the effects of the screening processes within cRPA (involving f orbitals from actinides, p orbitals from oxygen, and other orbitals)? (3) Is it mandatory to include the p orbitals among interacting orbitals? In this case, what is the influence of the starting electronic structure on the calculation of U^{ff} and U^{pp} ?

In this paper, we tackle these questions by extending the self-consistent calculation of U and J (within the DFT + U and cRPA schemes) of Refs. [33,34] to dioxides of actinides from neptunium to curium (in addition of uranium). (1) We first compute the effective f interaction within cRPA (as done in Ref. [36]): here, the effective interaction U^{ff} is found to be small for PuO_2 and much too small for AmO_2 and CmO_2 , even with self-consistency. Even if these results can be explained by the metallic character of the starting electronic structure, they remain unphysical. (2) Then, we show that cRPA screening processes between uncorrelated states (including those between p states from oxygen) are responsible for this behavior.⁴ We conclude that a suitable modeling of effective interactions in these systems requires to take into account both ff interactions and pp interactions as done in Ref. [35]. (3) Thus we perform additional calculations of all ff , fp , and pp interactions as in Ref. [35]. We extend their calculations to NpO_2 and AmO_2 . Moreover, we test the influence of the starting electronic structure (either GGA or GGA + U with $U = 2.0$ eV) on effective interactions in PuO_2 and CmO_2 and find that the effect is non-negligible, but does not change the physical picture. Thus we confirm that this modeling enables a consistent description of effective interactions and electronic structure.

This paper is organized as follows. First, Sec. II presents the scheme and computational details. Then, Secs. III and IV present the results, by considering the following procedure.⁵

(i) In Sec. III, we carry out an extensive determination of the electronic ground states in DFT + U for several values (up to 10.0 eV) of U —here, U is applied only to the f electrons; we denote it U^{ff} , and we will hereafter denote this electronic structure as DFT + U^{ff} . The occupation numbers and the values of gaps for actinide dioxides from UO_2 to CmO_2 are also discussed.

³Also, and interestingly, Kolorenč *et al.* argue that values of U suitable for description of experimental photoemission spectra for UO_2 should be much larger in DFT + DMFT than in DFT + U because of the difference of screening by oxygen states [26].

⁴We also study (in Appendix B) the influence of the localization of correlated wave functions on the computed values of U and J and find a weak effect.

⁵Here, (i) and (ii) correspond to the procedure used for lanthanides in Ref. [36].

(ii) Then, in Sec. IV, by considering only f electrons within the low-energy model, we perform cRPA calculations starting from the DFT + U^{ff} electronic structures for all values of U^{ff} , in order to find all possible self-consistent values of U . Also, we investigate the role of the various screening processes within cRPA on these results.

(iii) Then, still in Sec. IV, we include the p orbitals in the correlated subspace, and compute ff , fp , and pp interactions as in Ref. [35].

Appendix A discusses in more detail the number of f electrons and occupation matrices for DFT + U^{ff} calculations, and Appendix B studies the influence of the localization of correlated wave functions by comparing projected local orbital (PLO) and maximally localized (ML) Wannier functions on the values of U and J obtained in uranium dioxide.

II. METHODS AND COMPUTATIONAL DETAILS

Here, we describe the methods and computational details. We begin by an overview of the problem and the DFT + U /cRPA scheme used (Sec. II A), before defining in more detail the low-energy effective models investigated in this paper (Sec. II B). Then, we give the computational details (Sec. II D).

A. DFT + U /cRPA scheme

The exact resolution of the many body problem would require first to define a basis of orbitals, then to compute all fourfold indexed Coulomb integrals in this basis, and finally, to solve the resulting many body Hamiltonian. However, this is not possible for a solid : since the size of the Hilbert space is too large, the resolution of the many-body Hamiltonian is unfeasible in practice.

Thus a common choice is to restrict to the low-energy (near the Fermi level) degrees of freedom which are poorly treated at the LDA or GGA level—forming the correlated subspace, typically spanned by a set of local (“correlated”) orbitals for which the effective Coulomb interaction is large compared to the others. This correlated subspace, together with the interactions between the correlated orbitals, define the low-energy effective many body model, which can be solved, e.g., in DFT + U or DFT + DMFT.

Here, in the case of actinide dioxides, we focus on the “ f ” and “ p ” correlated subspaces formed by f -like states from actinides and p -like states from oxygen, respectively. We denote “ \tilde{r} ” the noncorrelated subspace, which encompasses all other states. We also denote r the subspace including both \tilde{r} and p .⁶ We compute the effective interactions between the correlated orbitals by using the DFT + U /cRPA scheme [33,36,37], which enables to investigate the self-consistency between the DFT + U electronic structure and the effective interaction computed from that electronic structure. The scheme is summarized as follows.

⁶Important technical details are (for both DFT + U and cRPA) (i) how to define these subspaces, (ii) how to build the orbitals spanning them, and (iii) how to ensure the consistency of the definition of orbitals between DFT + U and cRPA. These points will be discussed throughout Sec. II.

I. DFT + U^{ff}

We begin by computing the ground state within the DFT + U . In this work, we choose to apply the Hubbard term of DFT + U only on the subspace f , for which correlations are the most important. That is, the correlated subspace considered within DFT + U is always the f subspace, and the input parameters for DFT + U are U^{ff} and J^{ff} . We obtain the DFT + U^{ff} electronic structure.

2. cRPA effective interaction

Then, starting from the DFT + U^{ff} electronic structure, we define (i) the correlated subspace either only the f subspace or both f and p subspaces and (ii) how to build the orbitals spanning this correlated subspace.⁷

Then, we use the cRPA method in order to compute the effective interaction between the orbitals of the correlated subspace. This is done by taking into account the screening processes between all electrons, *except the screening processes of correlated electrons by themselves* [31]; since the latter screening effects will be treated within the solution of the exact many-body scheme (e.g., in DFT + DMFT) at a more accurate level. In RPA, screening processes are represented by electron-hole transitions between the occupied and unoccupied states of the starting electronic structure (here, DFT + U^{ff}), within the noninteracting polarizability $\chi_0(\omega)$. Among these transitions, the cRPA excludes those which are internal to the correlated subspace (i.e., between unoccupied and occupied correlated orbitals), yielding a constrained polarizability $\chi_0^c(\omega)$.

From the latter and the bare interaction v , the constrained dielectric matrix can be deduced by (in matrix notation) $\epsilon_r(\omega) = 1 - v\chi_0^c(\omega)$. We then invert the latter, yielding the screened interaction U as

$$U_{m_1, m_3, m_2, m_4} = \langle m_1 m_3 | \epsilon_r^{-1} v | m_2 m_4 \rangle \quad (1)$$

(where m_i are indices for correlated orbitals) from which U and J are computed [34].

B. Low-energy effective model

As outlined in the previous section, a crucial point is the choice of the low-energy model treated by the many-body solver, that is, which effective interactions have to be computed. In this paper, the low-energy model is built by choosing either only the f subspace or both f and p subspaces as the correlated subspace in cRPA, by using one of the models defined in the following.⁸

For each model, we notably give details about (a) the correlated subspace in cRPA (f or fp), (b) the definition of correlated orbitals spanning the correlated subspace in cRPA, and (c) how the cRPA screening is computed.

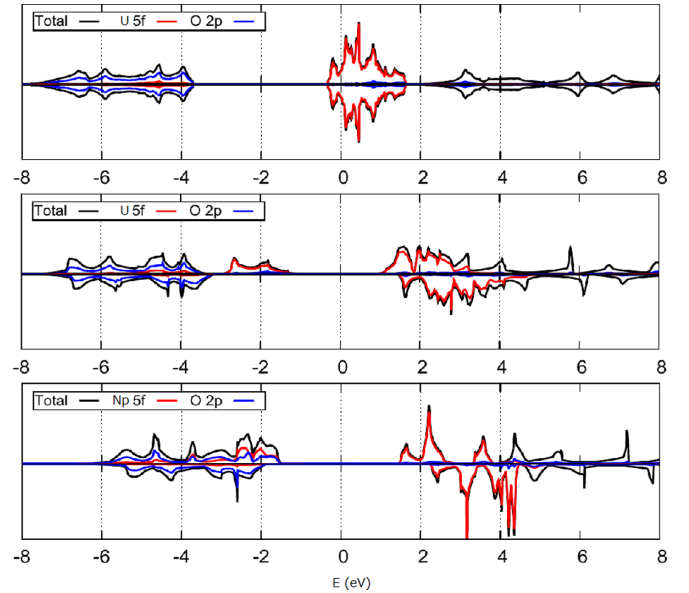


FIG. 1. Density of states for UO_2 in nonmagnetic GGA (top), UO_2 in ferromagnetic GGA + U^{ff} with $U^{ff} = 5.0$ eV and $J^{ff} = 0.57$ eV (middle), and NpO_2 in ferromagnetic GGA + U^{ff} with $U^{ff} = 5.0$ eV and $J^{ff} = 0.60$ eV (bottom). In each panel, upper/lower parts are the partial densities of states for spin up/down, respectively. The partial densities of states with $5f$ character from uranium/neptunium and $2p$ character from oxygen, for each spin, are also represented in red and blue, respectively. In the case of UO_2 in nonmagnetic GGA, hybridization between $5f$ and $2p$ densities of states is weak, so that all models defined in Sec. II B can be used. On the other hand, in ferromagnetic GGA + U^{ff} for UO_2 and NpO_2 , the f -like bands are mixed with high energy bands and also p -like bands from oxygen for NpO_2 so that ff and fp - fp models cannot be used in this case, and thus only f -ext model can be used.

1. f model (also called f - f)

This model can be used only in the particular case for which f -like bands from actinides (close to the Fermi level) are well separated from other bands, that is, they are not entangled with other bands⁹ (which is typically the case in nonmagnetic GGA for actinide dioxides, as in the upper panel of Fig. 1 for UO_2). (a) The correlated subspace in cRPA is f . (b) The correlated orbitals in cRPA are defined as projected local orbital (PLO) f Wannier functions¹⁰ [42] built from the f -like bands close to Fermi level. (c) The cRPA screening is computed by removing transitions among these correlated orbitals or, in this particular case, equivalently, f -like bands (ff transitions), keeping only the rr transitions and rf transitions.

⁹Still, let us denote that f -like bands close to the Fermi level may contain hybridization of f orbitals from actinides with other orbitals, including p from oxygen: this hybridization may be not negligible in general. In this case, the Wannier functions in the f - f model will have slightly mixed character (although f character will be dominant).

¹⁰For comparison, we also used ML Wannier functions [38–40] by using the WANNIER90 code [41] (see Appendix B) and find a rather weak effect.

⁷These definitions are discussed in detail in Sec. II B.

⁸The models considered in Sec. IV are f -ext and fp . The f - f and f - fp models will be used in Appendix B only.

Let us quickly describe the expression of the cRPA polarization. Given two of the subspaces among f , p , r , and \tilde{r} (denoted here as a and b), we define as $a \rightarrow b$ the screening channel gathering transitions between valence states in subspace a and conduction states in subspace b , and ab the union of $a \rightarrow b$ and $b \rightarrow a$ channels. By using these notations, the total RPA polarization is given by

$$\chi = \chi_{rr} + \chi_{rf} + \chi_{ff}, \quad (2)$$

in which the three terms (respectively χ_{rr} , χ_{rf} , and χ_{ff}), correspond to the three types of transitions participating to the screening (rr , rf , and ff), the constrained polarization is deduced as

$$\chi^r = \chi_{rr} + \chi_{rf}. \quad (3)$$

Then, the parameters U^{ff} and J^{ff} are deduced.

In this paper, the starting point of the cRPA in the f model is always the GGA nonmagnetic electronic structure, and self-consistency is not considered.

2. f - fp model

This model can be used in the same particular case than the f - f model, if we wish to check the effect of hybridization of f -like bands from actinides with p -like bands from oxygen (which is small, as seen in the upper panel of Fig. 1 for UO_2). (a) The correlated subspace in cRPA is still f . (b) The correlated orbitals in cRPA are still defined as PLO f Wannier functions, but, here, they are built from *both* f -like bands from actinides and p -like bands from oxygen. (c) The cRPA screening is computed by removing transitions among f states [as in Eq. (5)], either by selecting the band indices of the f -like bands [f - fp (a) model]¹¹ or by the weighting method [33,43,44] [f - fp (b) model]. Here, both choices are possible, since we are in the particular case of f -like bands not entangled with others. Then, the parameters U^{ff} and J^{ff} are deduced.

In this paper, as for the f - f model, the starting point of the cRPA in the f - fp model is always the GGA nonmagnetic electronic structure, and self-consistency is not considered. The main difference with respect to the f - f model is to increase slightly the localization of f orbitals, since the Wannier functions are built from more bands.

3. f -ext model

This model is an extension of the f - fp model in a more general case, that is, the f -like bands are not isolated from other bands—typically entangled with not only p -like bands from oxygen but also other bands (which is typically the case in GGA + U for actinide dioxides, as seen in the middle and lower panels of Fig. 1 for UO_2 and NpO_2), and/or

¹¹Here, an important remark is that f -like bands at Fermi level are *not* equivalent to the f PLO Wannier functions spanning the f subspace, which have character in both f -like and p -like bands. Thus, for the f - fp (a) model, there is a small inconsistency between the correlated subspace and the polarization. However, the inconsistency is small, as the PLO Wannier functions have only a weak weight in the p -like bands (see, e.g., the upper panel of Fig. 1 for UO_2).

the f character is shared between f -like, p -like, and other bands due to a stronger hybridization. (a) The correlated subspace in cRPA is still f . (b) The correlated orbitals in cRPA are still PLO f Wannier functions, defined from f -like bands, p -like bands, plus a few other bands above the f -like bands (which are entangled with the f -like bands). In practice, we use bands 5 to 28 (as in Ref. [33]). (c) The cRPA screening is computed by removing transitions among all selected bands by using the weighting coefficient method [33,43,44], the latter being mandatory here, since f bands are entangled with others. Then, the parameters U^{ff} and J^{ff} are deduced.

In this paper, the starting point of the cRPA in the f -ext model, is the GGA + U^{ff} electronic structure (in the f subspace, the correlated orbitals are built as atomic f orbitals), and we investigate self-consistency as described in Sec. II C.

4. f p model (also called fp - fp)

Here, we include the p degrees of freedom within the low-energy model, in addition of f degrees of freedom. (a) The correlated subspace in cRPA includes both f and p subspaces. (b) The correlated orbitals in cRPA are both PLO f Wannier functions and PLO p Wannier functions, built from both f -like and p -like bands.¹² (c) The cRPA screening is computed by removing all transitions within the subspace including both f and p subspaces. Here, we remove ff , pp , and pf transitions, keeping only the $\tilde{r}f$, $\tilde{r}p$, and $\tilde{r}\tilde{r}$ transitions. The total polarization in Eq. (2) is rewritten as

$$\chi = \chi_{\tilde{r}\tilde{r}} + \chi_{\tilde{r}p} + \chi_{pp} + \chi_{\tilde{r}f} + \chi_{pf} + \chi_{ff} \quad (4)$$

and the constrained polarization is

$$\chi^{\tilde{r}} = \chi_{\tilde{r}\tilde{r}} + \chi_{\tilde{r}f} + \chi_{rp}. \quad (5)$$

Then, the parameters U^{ff} , U^{fp} , and U^{pp} are deduced. Then, following the shell folding scheme derived in Ref. [35], one can compute renormalized interactions $\tilde{U}_{ff} = U_{ff} - U_{fp}$ and $\tilde{U}_{pp} = U_{pp} - U_{fp}$.

Here, an important question is the physical meaning of including the p orbitals inside the correlated subspace (b): since p -like bands are filled, is it necessary (and physically meaningful) to include their interaction? Here, two main reasons can be invoked.

First, the p -like bands contain self-interaction effects which need to be corrected as can be done in DFT + U [45]. These self-interaction effects have proven to be important in some oxides in recent studies (e.g., Refs. [46,47]).

Second, the p -like bands below Fermi level and f -like bands at Fermi level are not purely of p/f character, since they mainly result from the hybridization of p orbitals from oxygen and f orbitals from actinides. As a consequence, p orbitals are not filled and fluctuations can be important.

In practice, we use the fp model as follows: the starting point of the cRPA is either the GGA nonmagnetic structure,

¹²In this paper, we consider the fp model only for the GGA and GGA + U^{ff} electronic structures, with a low value of U^{ff} , so that bands above f -like bands remain disentangled from f -like bands.

TABLE I. Values of the fcc cell parameter a_{cell} within the fluorite crystal structure for dioxides of actinides from uranium to curium [51,52].

	UO ₂	NpO ₂	PuO ₂	AmO ₂	CmO ₂
a_{cell} (Bohr)	10.32	10.26	10.20	10.15	10.13

or the same GGA + U^{ff} electronic structure as for the f -ext model, with $U^{ff} = 2.0$ eV (here, we do not investigate self-consistency; we only check the difference between GGA and GGA + U^{ff} starting points).

C. Self-consistency between cRPA effective interaction and starting DFT + U^{ff} electronic structure in the f -ext model

Then, considering the cRPA effective interaction within the f subspace (that is, U^{ff} and J^{ff}) computed by using the f -ext model defined in Sec. II B 3, we compare it to the input values of U^{ff} and J^{ff} used for the DFT + U^{ff} calculation which was used by the cRPA as a starting point.

The DFT + U^{ff} /cRPA self-consistent scheme [33,36,37] does this comparison for several input values of U^{ff} and J^{ff} , in order to compute self-consistently the electronic structure within DFT + U^{ff} , and the effective interaction parameters U^{ff} and J^{ff} within cRPA. Self-consistent values of U^{ff} and J^{ff} are obtained when the output and input values are equal.

In order to preserve self-consistency, we check the coherence between the correlated wave functions used in DFT + U^{ff} (atomic orbitals), and those used in cRPA (PLO Wannier functions). To do so, we compute the diagonal bare interaction calculated in the atomic orbitals basis and in the PLOWF basis. As discussed in Refs. [48,49], the considered atomic orbitals are, in practice, truncated at the PAW radius, then the density matrix is renormalized. We checked that the value of bare interaction computed with Wannier functions, is close to the value of the bare interaction computed either with true atomic wave functions or renormalized atomic wave functions. The maximal difference is 1.8 eV. It should thus impact the values of effective interactions, which are more than 4 times smaller, by ~ 0.5 eV.

D. Computational details

1. Physical parameters

Dioxides of actinides from uranium to curium present a fluorite-type crystal structure [50–52], in which actinide atoms form a face-centered cubic (fcc) lattice, whose tetrahedral interstitial sites are occupied by oxygen atoms. Values of cell parameters are gathered in Table I. As the structure has cubic symmetry, we use in the determination of occupation matrix in DFT + U^{ff} the cubic real spherical harmonics (CRSH) basis, as in Ref. [36].

According to experiment, actinide oxides are paramagnetic at ambient temperature [53–57], although an antiferromagnetic (AFM) ordering may appear at sufficiently low temperatures [56,58,59]. However, the DFT + U method is hampered by the creation of an artificial magnetism even for systems which are paramagnetic, and also by the problem of metastable states [21,24], due to the different possibilities

for the electrons to occupy the correlated orbitals. Here, we consider the ferromagnetic (FM) ordering in DFT + U^{ff} for the sake of simplicity. In order to determine the DFT + U^{ff} ground state in this ordering, we use the procedure discussed in Ref. [36]: we consider all possible filling of the diagonal elements of the occupation matrix in the CRSH basis and determine the most stable configuration.

2. Computational conditions and convergence parameters

For DFT and DFT + U calculations, we use the GGA/PBE functional [9] (with spin polarization, without spin-orbit coupling) and the implementation of DFT + U and cRPA within ABINIT [33,48]. Calculations are performed by using the PAW formalism [60], as implemented in ABINIT [61]. The PAW atomic data for actinides includes $6s$, $6p$, $7s$, $5f$, and $6d$ electrons as the valence electrons, whereas for oxygen, we consider $2s$ and $2p$ electrons as the valence electrons. Concerning the plane waves cutoff used in the calculation, we use 15 Ha for the wave functions, 60 Ha for compensation quantities in PAW, 5 Ha for polarization, and 35 Ha for the plane-wave decomposition of matrix elements of the cRPA effective interaction (see Appendix C of [36] for more details). Also, we use 100 bands for the cRPA polarization, 64 k points to sample the full Brillouin zone, and a Fermi-Dirac smearing of 0.1 eV.

3. Self-consistency

In each iteration of the self-consistent cRPA scheme, we observe in practice (as discussed in Ref. [36]) that the output value J_{out}^{ff} of J^{ff} depends weakly on the input value U_{in}^{ff} of U^{ff} ,¹³ so that the self-consistent calculation of J^{ff} can be done at a fixed input value U_{in}^{ff} of U^{ff} , separately from the self-consistent calculation of U^{ff} . We use the same procedure here.

III. RESULTS: GGA + U^{ff} ELECTRONIC STRUCTURE

We discuss first the results concerning the ground states obtained within the GGA + U^{ff} calculations. As mentioned in Sec. II D 1, the use of DFT + U requires to determine the ground state in terms of orbital occupations in the CRSH basis. Here, we discuss first this determination. Then, using the ground state for each oxide, we describe the band gaps obtained in comparison to other studies.

A. Determination of the GGA + U^{ff} ground state and occupations of f orbitals

In order to compute self-consistent values of U^{ff} , a first step is to find the GGA + U^{ff} ground state as a function of the input value U^{ff} (denoted hereafter as U_{in}^{ff}). In the literature, the GGA + U^{ff} ground state was determined for realistic values of U_{in}^{ff} , by using an occupation matrix control scheme [21,22,24,25,28,62,63] in order to deal with the occurrence

¹³As an example, for AmO₂, the variation of J^{ff} between a GGA and a GGA + U calculation is less than 0.02 eV.

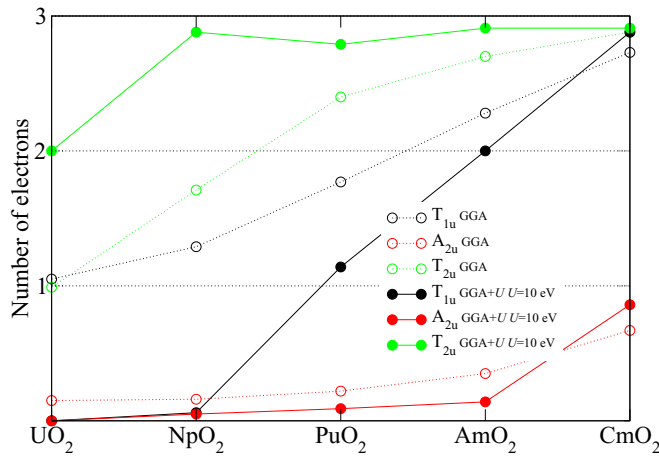


FIG. 2. Occupations of T_{1u} , A_{2u} , and T_{2u} orbitals for actinide dioxides, in GGA and GGA + U^{ff} (for $U^{ff} = 10$ eV). In GGA, all occupations increase for one actinide to the next. In GGA + U^{ff} , only one of the orbitals increases its occupations for one actinide to the next.

of metastable states [64]. Here, we extend this study for all values of U_{in}^{ff} from 0 to 10 eV.¹⁴

The GGA + U^{ff} ground states are described by the occupation matrix in the CRSH basis as a function of U^{ff} , given in Table VII in Appendix A2 for each oxide. Occupations are also plotted in (i) GGA and (ii) GGA + U^{ff} with $U^{ff} = 10$ eV, for all actinide dioxides, in Fig. 2.

Here, we discuss more specifically Fig. 2. In GGA, we first observe a change in the order of orbital occupations when increasing the atomic number of the considered actinide: indeed, for UO_2 , we see that T_{1u} orbitals are slightly more filled, followed by T_{2u} , then A_{2u} orbitals. On the contrary, from NpO_2 to CmO_2 , the T_{2u} orbitals become the most filled, followed by T_{1u} , then A_{2u} orbitals. Concerning the general tendency of GGA occupations as a function of the atomic number of the considered actinide, the important points are that (i) occupations respect orbital degeneracies and (ii) all occupations increase concomitantly along the line.

In contrast, as discussed earlier [21,24,64], GGA + U requires most often to break the cubic symmetry, depending on the number of electrons and the degeneracy of orbitals, e.g., for UO_2 , PuO_2 , AmO_2 ¹⁵ (see Table VII in Appendix A2). Also, in contrast to the GGA case, the occupations do not increase concomitantly along the line, but instead, from a given oxide to the following one, one of the occupations increases by (almost) one, except for CmO_2 , for which two occupations increase by (almost) one, attempting to fill the $5f$ shell. For example, from UO_2 to NpO_2 , only the electron number inside the T_{2u} subspace increases, in agreement with the fact that the electron interaction energy has to be minimized (the interaction energy is less important if the electron

density is not shared among different orbitals). This description is valid for large values of U^{ff} (10 eV) (see Table VII in Appendix A2). For intermediate values of U^{ff} , for UO_2 , another low-symmetry configuration appears, which results from the hybridization between two orbitals (see Appendix A2 for the peculiarities of the evolution of occupations as a function of U^{ff}).

B. Band gaps

Here, we discuss the band gaps obtained from the GGA + U^{ff} ground states discussed in Sec. III A. Indeed, before proceeding any further, an important point is to compare these band gaps to the literature, since (i) we neglect SOC and we restrict to the ferromagnetic case and (ii) the band gap plays an important role on the screening properties.

The latter point might be surprising, since, e.g., for UO_2 , the band gap separates f -like bands both in the valence and conduction bands, and, moreover, transitions between f orbitals are suppressed from the cRPA polarizability. However, when the PLO f Wannier functions in cRPA are built not only from f -like bands but also other bands (as in the f -ext model), f -like bands are not purely of f character, and contain also p character since they contain f orbitals hybridized with oxygen p orbitals. Thus transitions between occupied and empty f -like bands include not only the ff screening channel excluded from the cRPA polarizability, but also the fp screening channel taken into account in the cRPA polarizability. Thus band gaps are important for the screening, even in cRPA.

Here, we compare our results to other DFT + U^{ff} calculations on actinide dioxides in the literature on Ref. II. Two important remarks are to be done concerning the latter. (1) They generally use values of U_{in}^{ff} close to 5.0 eV [21,22,24,25,28]. Thus this latter value can be, in our case, considered as a test value enabling to discuss our GGA + U^{ff} calculations, at least qualitatively. (2) They are often performed in the antiferromagnetic (AFM) phase instead of the ferromagnetic (FM) phase, in order to reproduce more correctly the experimental magnetic ordering at low temperature.

Considering the previous points, we compare our values of the gap in both FM and AFM phases, denoted respectively E_g^{AFM} and E_g^{FM} —for GGA + U^{ff} calculations with $U_{in}^{ff} = 5.0$ eV and $J_{in}^{ff} = J_{SC}^{ff}$ given in Table IV—to those obtained in Refs. [21,22,24,25,28]. All these values are given in Table II, along with experimental values [2,65,66]. We comment them in the following.

(1) UO_2 . We obtain $E_g^{FM} = 1.75$ eV and $E_g^{AFM} = 2.55$ eV, surrounding the experimental value from [65] (2.1 eV). This is in good agreement with the literature, though values of U_{in}^{ff} are not exactly the same (see, e.g., Refs. [21,28]). However, Ref. [28] shows that SOC increases the gap by 0.4 eV.

(2) NpO_2 . The experimental value of the gap (2.85 eV from Ref. [2]) is well reproduced by our results in both FM and AFM phases. Agreement with other calculations is also good. Also, the value of E_g^{AFM} obtained in [22] for $U_{in}^{ff} = 5.0$ eV and $J_{in}^{ff} = 0.51$ eV is close to ours. Again, Ref. [28] highlights the role of SOC on the gap (0.15 eV).

¹⁴Once the ground state is found for a given value of U_{in}^{ff} (see Table VII in Appendix A2), we compute the output values U_{out}^{ff} of U^{ff} within cRPA, as a function of the input values U_{in}^{ff} used in the GGA + U^{ff} calculations. This will be discussed in Sec. IV.

¹⁵Of course, spin orbit coupling would change this picture.

TABLE II. Values of the band gap (in eV) for actinide dioxides: experiment from Refs. [2,65]. It was often assumed in literature that Ref. [66] gives experimental gaps for NpO_2 and AmO_2 , it appears indeed that the number given (3.1 and 1.3 eV) are instead results from *ab initio* calculations. Our calculations in the ferromagnetic (FM) and antiferromagnetic (AFM) phases are indicated by \dagger and use $U_{\text{in}}^{ff} = 5.0$ eV, $J_{\text{in}}^{ff} = J_{\text{SC}}^{ff}$ given later in Table IV. Results from other calculations [21,22,24,25,28,67] (DFT + U^{ff}) are also reproduced. The GGA functional used is the PBE variant, except for Ref. [22]. For the DFT + U^{ff} calculations, spin-orbit coupling (SOC) is taken into account only in Refs. [25] and [28].

Method			UO_2	NpO_2	PuO_2	AmO_2	CmO_2
Exp. [65]			2.1				
Exp. [2]				2.85	2.80		
This work	U_{in}^{ff}	J_{in}^{ff}	UO_2	NpO_2	PuO_2	AmO_2	CmO_2
GGA + $U^{\text{FM}\dagger}$	5.0	J_{SC}	1.8	2.9	1.5	0.1	0.0
GGA + $U^{\text{AFM}\dagger}$	5.0	J_{SC}	2.6	3.1	2.2	0.8	0.0
Literature DFT + U (AFM)							
GGA + U [21]	4.5	0.51	2.4				
GGA + U [22]	5.0	0.51		2.9			
GGA + U [24]	4.0	0.7			2.2		
GGA + U [66]	5.0	0.0		3.1		1.3	
GGA + U [67]	5.0	0.75				0.7	
GGA + SOC + U [25]	5.0	0.75				1.4	
LDA + U [28]	4.0	0.0	1.9	2.2	1.5	0.0	0.0
LDA/SOC + U [28]	4.0	0.0	2.3	2.4	2.1	1.0	0.1
Literature DFT+DMFT (PM) [26]							
LDA/SOC+DMFT	6.5	0.7	1.9	2.5	2.5		
Literature hybrid functionals (AFM)							
HSE/SOC [15,68]			2.4	2.4	2.6	1.5	0.4/1.0

(3) PuO_2 . For the FM phase, we obtain $E_{\text{g}}^{\text{FM}} = 1.45$ eV, which is low compared to the recent reevaluation of the experimental value (2.80 eV [2]). For the AFM phase, our value is a bit closer ($E_{\text{g}}^{\text{AFM}} = 2.2$ eV), but still low. Values of the band gap in the literature [24,28] obtained with lower values of U_{in}^{ff} are also underestimated. This suggests that a higher value of U_{in}^{ff} is necessary for a correct description of the gap. Also, SOC has been shown to have an important effect on the gap (0.6 eV) [28].

(4) AmO_2 . We obtain $E_{\text{g}}^{\text{FM}} = 0.1$ eV. For the AFM phase, our value is a bit larger ($E_{\text{g}}^{\text{AFM}} = 0.8$ eV). According to Refs. [25,28], SOC has a large effect on the band gap, which becomes larger by using $U_{\text{in}}^{ff} = 5.0$ eV and $J_{\text{in}}^{ff} = 0.75$ eV [25].

(5) CmO_2 . We find a metallic state (zero gap) in both FM and AFM phases. This is the same for $U_{\text{in}}^{ff} = 4.0$ eV and $J_{\text{in}}^{ff} = 0.0$ eV (LDA + U_{in}^{ff}) without SOC [28]. Nonetheless, the gap becomes nonzero by taking into account the SOC [28].

C. Discussion

These results suggest that, for values of U_{in}^{ff} close to 5.0 eV, the roles of both SOC and AFM ordering have in

TABLE III. Values of the diagonal elements of the bare interaction in the Wannier basis, for dioxides of actinides from uranium to curium.

	UO_2	NpO_2	PuO_2	AmO_2	CmO_2
$U_{\text{bare}}^{\text{diag}}$ (eV)	17.57	19.21	19.55	20.35	21.33

general a non-negligible effect on the value of the band gap for the LDA/GGA + U_{in}^{ff} electronic structure (except for CmO_2 , in which the non-negligible effect is confirmed only for the SOC, and NpO_2 , for which AFM ordering plays a minor role). However, we denote that another study [15], using the hybrid functional HSE instead of LDA/GGA, concludes that the role of SOC on the band gap is weak for actinide oxides. Lastly, we emphasize that these studies do not discuss a complete search of the DFT + U_{in}^{ff} electronic ground state, at the exception of Refs. [21,24,67], raising questions on the reliability of the ground state since the state with the largest gap is not always the ground state [21].

Thus both SOC and magnetic ordering might have an influence on the screening processes. The case of magnetic ordering will be briefly discussed in Sec. IV.

IV. RESULTS: CRPA EFFECTIVE INTERACTION

In this section, we briefly discuss the bare ff interaction in GGA (Sec. IV A) and values of J^{ff} (Sec. IV B), before presenting the main outcome of the paper: (a) in Sec. IV C, self-consistent calculation of U^{ff} within the f -ext model and (b) in Sec. IV D, calculations of U^{ff} , U^{fp} , and U^{pp} —

TABLE IV. Self-consistent values J_{SC}^{ff} of J^{ff} (in eV) found for actinide dioxides within the DFT + U /cRPA scheme, compared to values from Ref. [5].

	UO_2	NpO_2	PuO_2	AmO_2	CmO_2
This work: J_{SC}^{ff} (eV)	0.57	0.60	0.63	0.67	0.70
Kotani <i>et al.</i> [5]	0.54	0.61	0.68	0.75	0.82

necessary for the shell folding scheme of Ref. [35]—within the fp model. In Sec. IV E, we discuss the comparison of results within both f -ext and fp models, and with respect to the literature.

A. Bare interaction in GGA

Starting from the GGA electronic structure, bare interactions in the basis of Wannier functions are given in Table III for each oxide. They depend weakly on the exchange and correlation, since the screening is not involved in the calculation of bare interactions, so that bare interactions computed in GGA and in GGA + U^{ff} are very close (the difference is smaller than 0.1 eV). The values of bare interactions increase from UO_2 to CmO_2 , reflecting the tendency towards localization of orbitals when the charge of the nuclei of the considered actinide atoms is increased.

B. Calculation of J^{ff}

In order to compute, the values of J^{ff} (in accordance with the discussion in Sec. II D 3), we start from the initial conditions $U_0^{ff} = 7.0$ eV and $J_0^{ff} = 0.6$ eV, and carry out a self-consistent calculation of J^{ff} .

Results are gathered in Table IV, along with values of Ref. [5]. We observe that our self-consistent values of J^{ff} increase progressively with the atomic number, which can be interpreted by the progressive contraction of $5f$ atomic orbitals around the nuclei of actinide atoms when increasing their atomic number, leading to stronger exchange interactions. Values from [5] are close to ours, although their increase is a bit faster (there is a shift of 0.12 eV for curium dioxide). Values obtained by Ref. [23] (0.5–0.6 eV) are slightly lower than ours.

C. Effective interaction as a function of U_{in}^{ff} and self-consistent values in the f -ext model

1. Calculation of U^{ff}

We now present the values of the cRPA interaction obtained within the f -ext model. More precisely, we focus on the curve $U_{\text{out}}^{ff}(U_{\text{in}}^{ff})$, where U_{out}^{ff} is obtained from the cRPA calculation starting from the electronic ground states obtained in GGA + U^{ff} for a given value of U_{in}^{ff} . Results are gathered in Fig. 3. We observe three different qualitative behaviors. (1) First, for UO_2 , NpO_2 , and PuO_2 , the curve $U_{\text{out}}^{ff}(U_{\text{in}}^{ff})$ increases significantly before crossing the black line ($U_{\text{out}}^{ff} = U_{\text{in}}^{ff}$) for $U^{ff} \simeq 5$ eV, after which the curve increases more slowly. Thus a unique self-consistent value is obtained. (2) Second, for AmO_2 , U_{out}^{ff} remains almost constant between 1 and 2 eV and crosses the bisection line. For larger values of U^{ff} , the increase is more important, but the curve does not cross the black line, so that a unique low self-consistent value ($U_{\text{SC}}^{ff} = 1.4$ eV) is obtained. (3) Finally, for CmO_2 , U_{out}^{ff} increases slowly and erratically. A unique low self-consistent value is also obtained.

In the next section, we will analyze these curves in term of screening processes. But first, and in order to validate furthermore this approach, we did, for the case of AmO_2 , a cRPA calculation for both AFM and FM configurations for $U_{\text{in}} =$

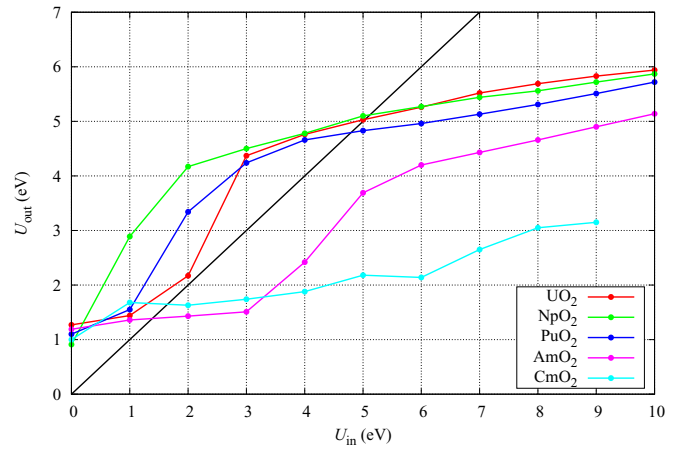


FIG. 3. Output values U_{out}^{ff} of U^{ff} obtained within cRPA as a function of the input values U_{in}^{ff} used in the DFT + U^{ff} calculations

5 eV. We found a small increase of U_{out} (0.4 eV). Although non-negligible, this is not sufficient to change significantly the physical picture of Fig. 3.

2. Screening processes in the f -ext model

We discuss here in more details the screening processes involved in the results detailed in Sec. IV C 1 concerning the f -ext model. The main result of this section is that transitions between states which are *not* considered as correlated within the f -ext model, are responsible for the low values of U^{ff} in AmO_2 and CmO_2 , since these systems are described to have a small gap or are metallic.

(a) *Partially screened effective interactions.* Among the screening processes discussed in Sec. II B, we study here those between electrons which are not considered as correlated within the f -ext model, that is, within the r subspace including both \tilde{r} and p subspaces (rr channel). These processes are especially important in AmO_2 and CmO_2 , due to the small band gaps in these systems (see Sec. III B).

The (averaged) partially screened interaction $U_{\text{only } rr}^{ff}$ —computed by using a modified constrained polarization, including only the rr screening—is plotted on Fig. 4.

Here as well, three different behaviors are observed.

(1) For UO_2 , NpO_2 , and PuO_2 , $U_{\text{only } rr}^{ff}$ is nearly constant (at around 8 eV), decreasing weakly below $U_{\text{in}}^{ff} = 3.0$ eV. This slight decrease may be due to the increase of the hybridization between f and r densities of states for low values of U_{in}^{ff} .

(2) For AmO_2 , $U_{\text{only } rr}^{ff}$ decreases between $U_{\text{in}}^{ff} = 0.0$ and 3.0 eV, then increases again between $U_{\text{in}}^{ff} = 3.0$ and 6.0 eV, before stabilizing at the same values than for UO_2 , NpO_2 and PuO_2 . We interpret the behavior between $U_{\text{in}}^{ff} = 0.0$ and 6.0 eV as the effect of a stronger hybridization between f and r densities of states, when the f -like bands go progressively into the p -like bands. Because of this, part of the r density of states (p density of states from oxygen) goes above the Fermi level, which increases significantly the contribution of rr transitions to the constrained polarization. We denote that for AmO_2 , both $U_{\text{only } rr}^{ff}$ (Fig. 4) and U_{out}^{ff} (Fig. 3) begin to increase at $U_{\text{in}}^{ff} = 3.0$ eV. This suggests rr screening is

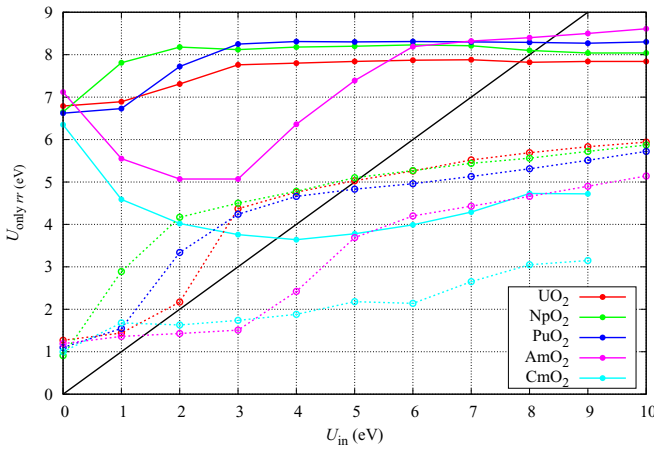


FIG. 4. Values of $U_{\text{only } rr}^{ff}$ obtained within cRPA, as a function of the input values U_{in}^{ff} used in the DFT + U^{ff} calculations. The output values U_{out}^{ff} of U^{ff} from Fig. 3 are reproduced in dotted lines for comparison

responsible for the different behavior of the U_{out}^{ff} (U_{in}^{ff}) curve for AmO₂, with respect to UO₂, NpO₂, and PuO₂.

(3) For CmO₂, $U_{\text{only } rr}^{ff}$ decreases strongly between $U_{\text{in}}^{ff} = 0.0$ eV and $U_{\text{in}}^{ff} = 4.0$ eV, before increasing slightly up to 8.0 eV. This is interpreted as the effect of an even stronger hybridization between f and r densities of states. For values superior to $U_{\text{in}}^{ff} = 8.0$ eV, $U_{\text{only } rr}^{ff}$ stabilizes at $\simeq 4.7$ eV, far below the values for the other dioxides. This is interpreted as the consequence of the presence of r density of states above the Fermi level, even when hybridization between f and r states vanishes at high values of U_{in}^{ff} . Indeed, the system is still a metal even for large values of U_{in}^{ff} .

To summarize, the rr screening is the cause of the qualitative behavior of the U_{out}^{ff} (U_{in}^{ff}) curve for AmO₂ and CmO₂, which prevents the obtention of a unique and high self-consistent value of U^{ff} for these dioxides. This raises several points.

First, this rr screening might be due to the small values of the gap found in these two systems. As we discussed above, SOC and AFM could increase these values. Concerning the possible role of AFM ordering, as discussed previously in the case of AmO₂, it is not sufficient to change significantly the physical picture.

Second, one could also argue that a better description of correlation—for instance, by using DFT + DMFT instead of DFT + U^{ff} —could improve the density of states or spectral function. However, and as outlined in Ref. [36], using DFT + DMFT instead of DFT + U^{ff} is not expected to change the qualitative results for AmO₂ and CmO₂, because there would be possibly more f spectral weight near the Fermi level, which is expected to increase the screening, and thus, reduce further the output values of U^{ff} . Thus we choose to focus on the GGA + U^{ff} electronic structure.

Third, in Ref. [69], a system in which two types of orbitals are correlated (such as the f and the p orbitals in our case) was studied. It was shown that cRPA, when considering only the f subspace as correlated, does not yield good results. Indeed,

U^{ff} does not lead to a spectral function in agreement with the one computed within the full model. This is in agreement with the present study: U^{ff} does not describe well the true spectral function. As discussed in Ref. [69], it can be expected, since the cRPA dielectric function does not describe the fact that interacting p electrons are more localized, so that they should participate less in screening processes. They propose to compute effective interaction by using a more accurate response function computed directly in DMFT. Another solution is to compute all interactions among all correlated orbitals as in Ref. [35], in order to build the equivalent of the full model of Ref. [69]. This is the goal of the next section.

D. Calculations in the fp model

Here, we carry out cRPA calculations of U^{ff} , U^{fp} and U^{pp} in the fp model, and apply the same shell folding scheme as in Ref. [35] (briefly discussed in Sec. II B).

Results are gathered in Table V [line (e)]. Self-consistency will be discussed in Sec. IV E; here, we discuss more specifically the comparison between the values of U^{ff} , U^{fp} , and U^{pp} obtained here and in Ref. [35] [line (d)].

We see that U^{fp} and U^{pp} are somewhat different (respectively ~ 0.4 – 0.5 eV larger and ~ 0.8 – 0.9 eV smaller) in comparison to results of Ref. [35]. On the other hand, the values of U^{ff} are very close (difference is ~ 0.1 eV). Moreover, the variation of U^{ff} as a function of the actinide is very similar and increases smoothly from UO₂ to CmO₂. Our calculations for NpO₂ and AmO₂—that were not done in Ref. [35]—confirm this variation.

However, all these cRPA calculations start from the GGA electronic structure (LDA results are very close, within 0.2 eV), and the LDA/GGA metallic densities of states are not correct. And, we know, according to the work of Kotani *et al.*, that a correct electronic structure is obtained by using large values of U^{ff} . Thus, in addition, we tested the dependency of the results for the fp model with respect to the input electronic structure. In order to do so, we computed U^{ff} and U^{pp} by starting from a GGA + U^{ff} electronic structure with $U_{\text{in}}^{ff} = 2$ eV,¹⁶ for PuO₂ and CmO₂. We found a rather small variation of U^{ff} (0.3 eV for PuO₂) and U^{pp} (0.1 eV for PuO₂). In comparison, for the f -ext model, going from $U_{\text{in}}^{ff} = 0$ to 2 eV increases the value of U^{ff} computed for PuO₂ by 2.3 eV (see Fig. 3).

A fully self-consistent calculation within the fp model would require to have input values for *both* U^{ff} and U^{pp} in DFT + U , which is beyond the goal of this study. However, it is expected that the main effect on the electronic structure (especially near the Fermi level) is induced by U^{ff} , since f orbitals are the closest to the Fermi level, and the most important transitions in the polarizability involve the states near the Fermi level. This suggests that a fully self-consistent calculation of U^{ff} and U^{pp} (with input values of U^{ff} and U^{pp}) would lead to close results.

¹⁶A larger input value of U^{ff} would entangle the f -like bands with bands higher in energy, which would complicate the comparison.

TABLE V. Values U_{out} of U (in eV) found for actinide dioxides within several schemes. (a) Kotani [5] extracted values of U^{ff} from experiment using an Anderson model. These values are the reference values that a given method should obtain to be able to describe these systems. [(b) and (c)] Values obtained in this work without self-consistency ($U_{\text{in}}^{ff} = 0$) and with self-consistency. They highlight that, within this model, self-consistency is necessary and sufficient in order to have a good description of UO_2 and NpO_2 , but not sufficient for other oxides (see also Refs. [33,34]). [(d)–(g)] Seth *et al.* have done calculations of U^{ff} and U^{pp} by using a fp - fp model and a shell folding (SF) scheme without self-consistency. We have reproduced these calculations (see also text), which give results comparable to experiment. So, within the fp - fp model, self-consistency is not required. (h) Nonetheless, we test the possible impact of self-consistency for PuO_2 and CmO_2 , by using a nonzero input value $U_{\text{in}}^{ff} = 2.0$ eV. We see that values of U^{ff} and U^{pp} are only slightly modified. (i) Self-consistent GW calculations [23] give larger values of U^{ff} , somewhat in agreement with calculations of Seth *et al.* [line (d)] but without the shell folding scheme. See main text for discussion.

Method	U_{in}^{ff}	cRPA model	UO_2			NpO_2			PuO_2			AmO_2			CmO_2					
			ff	pp	pf	ff	pp	pf	ff	pp	pf	ff	pp	pf	ff	pp	pf			
Extracted from experiment																				
(a) Kotani <i>et al.</i> [5]	Experiment		4.5			5.0			5.5			6.0			6.7					
cRPA for ff interactions																				
(b) This work	cRPA	0.0	f -ext			1.2			0.9			1.1			1.2					
(c) This work	cRPA	U_{out}	f -ext			5.0			5.1			4.8			1.4					
cRPA for ff , pp , and pf interactions																				
(d) Seth <i>et al.</i> [35]	cRPA (no SF)	0.0	fp			6.5	6.0	1.9	7.3			6.3	2.0	8.0			6.7	2.1		
(e) This work	cRPA (no SF)	0.0	fp			6.4	5.1	2.3	6.9	5.3	2.4	7.2	5.5	2.5	7.6	5.7	2.6	7.9	5.8	2.6
(f) Seth <i>et al.</i> [35]	cRPA + SF	0.0	fp			4.6	4.1		5.3			4.3	5.9			4.6				
(g) This work	cRPA + SF	0.0	fp			4.1	2.8		4.4	2.9		4.7	3.0	5.0	3.1		5.3	3.2		
(h) This work	cRPA + SF	2.0	fp						5.0			2.9	5.4			3.1				
Self-consistent GW and calculations of ff interactions																				
(i) Yin <i>et al.</i> [23]	GW (RPA)	0.0	6.0			6.3			6.5			7.0			7.4					

E. Discussion

Here, we compare our self-consistent values U_{SC}^{ff} obtained in the f -ext model to the values obtained in the fp model (in this work and in Seth *et al.* [35]), and to the values obtained by self-consistent GW [23].

These are gathered in Table V, compared to U^{ff} obtained from experiment by Kotani *et al.* [5] [line (a) in Table V].

First, we remind how Kotani *et al.* [5] obtained these values. They estimated U^{ff} by comparing 4 f -XPS spectra obtained from the solution of the Anderson model and experiment. Concerning J^{ff} , according to Ref. [70] cited in Ref. [5], it was “translated from the Racah parameters E_1 , E_2 and E_3 fitted to optical data and photoemission of the actinide oxides.”

Then, we begin by comparing cRPA results in both this work and in Ref. [35], without shell folding [lines (b)–(e) in Table V]. Calculations of U^{ff} from the GGA band structure, in the f -ext model [line (b) in Table V], lead to very small values of U^{ff} (around 1 eV). Such low values are mainly due to the screening created by pp and pf transitions around the Fermi level (see Sec. IV C 2), because of the hybridization. As shown in Figure 3, for larger values of U_{in} , U^{ff} increases—in particular for UO_2 , NpO_2 and PuO_2 —, and is much larger, since these systems are insulating in GGA + U^{ff} for large U^{ff} . For UO_2 , NpO_2 and PuO_2 , the self-consistent values U_{SC}^{ff} of U^{ff} [line (c) in Table V] are in correct agreement with the range expected in order to reproduce the experimental photoemission spectra [5]. For UO_2 , our self-consistent value is identical to the one found in Refs. [33,34] (5.0 eV), which was calculated within a similar cRPA scheme but with a different occupation matrix, and lower than the one found in the

fp model either in this work or in Ref. [35] [6.5 and 6.4 eV, see lines (d) and (e) on Table V]. Also, for NpO_2 and PuO_2 , the self-consistent value in the f -ext model is much smaller than the one found in the fp model. For all these systems (UO_2 , NpO_2 , and PuO_2), the difference between U^{ff} in the two models is simply due to the fact that the fp screening is present in the f -ext model, but not in the fp model. However, for these three systems, after applying the shell folding, the renormalized value of U^{ff} , namely, $U^{ff} - U^{pf}$, is close to the self-consistent results obtained in the f -ext model. The latter fact is a coincidence, since the physical origin of this reduction is not the same: in the shell folding scheme for the fp model, it comes from the renormalization by intershell interaction between f and p electrons, whereas in the f -ext model, it comes from the fp screening. However, for AmO_2 and CmO_2 , the obtained values in the f -ext model (either self-consistently or for $U_{\text{in}}^{ff} = 5$ eV) are far below those expected in order to reproduce the experimental photoemission spectra [5], as well as those obtained in the fp model. This is due to the fact that these systems have small gaps (or are metallic) in DFT + U^{ff} , so that the screening is larger in the f -ext model, since this model is sensitive to what occurs at the Fermi level as explained above.

Thus we find that the f -ext model fails to give values of U^{ff} in accordance with the data calculated from experiment in Kotani *et al.* [5], suggesting that the model should be extended by using more correlated orbitals. The origin of this failure in terms of screening has been discussed in Sec. IV C 2. On the other hand, the fp model combined with the shell folding scheme gives values of U^{ff} much closer to those in Kotani *et al.* [5].

We now compare our calculations in the f -ext model to results obtained with the self-consistent GW approach. These calculations lead to high values of U^{ff} . This may seem surprising, since the screening is computed in RPA and not in cRPA, and a naïve expectation is that the screening should be larger in RPA, so that U^{ff} should be smaller. However, it was shown in Ref. [33] that for a DFT + U^{ff} (insulating) band structure of UO_2 , fully screened (RPA) interaction and cRPA effective interaction within the f -ext model are close, since the ff screening is very weak. So, the difference between cRPA and RPA is not the origin of the difference between our values and those obtained within the self-consistent GW approach, provided the system is insulating as in DFT + U^{ff} . Furthermore, it was shown [15] that hybrid functionals—which yield results close to GW calculations—lead to insulating solutions with rather large gaps (from 2.4 eV for UO_2 to 1.5 eV for AmO_2 [15]). Thus self-consistent GW calculations of Ref. [23] probably lead as well to insulating solutions, for which cRPA and RPA calculations are similar. This seems to be confirmed for UO_2 by a recent partial self-consistent GW calculation [71]. In order to refine furtherly this analysis, let us outline that in GW [71] and hybrid functional [15] calculations, oxygen p states are lowered in energy in comparison to DFT + U^{ff} , since DFT + U^{ff} acts only on f orbitals whereas GW acts on all orbitals. This is shown in Ref. [71] for UO_2 , and discussed in Refs. [15,68] for hybrid functionals (which should give close results to GW calculations). As a consequence, pf screening arising from GW electronic structure should be lower than pf screening arising from DFT + U^{ff} , which may explain why GW leads to higher values of U^{ff} in comparison to those computed in the f -ext model.

Finally, we compare the self-consistent GW calculations with our cRPA calculations within the fp model. In this case, the difference between cRPA and GW (RPA) screening is not negligible, since the large fp screening is suppressed in the fp model within cRPA, but kept in GW (RPA). As a consequence, U^{ff} is larger in cRPA (within the fp model before shell folding) than in GW (RPA).

V. CONCLUSION

We have computed the effective interaction between correlated electrons for actinide dioxides (within the cRPA scheme), by choosing the correlated subspace as either (a) the f orbitals from actinides, or (b) both f orbitals from actinides and p orbitals from oxygen. We have studied more particularly the effect of self-consistency over the effective interaction U^{ff} between f electrons—between the starting GGA + U^{ff} electronic structure and the cRPA calculation—and the effect of the inclusion of p orbitals within the correlated subspace. The main results—answering the three questions in the introduction—are summarized as follows.

(1) By choosing the correlated subspace as the f subspace, cRPA values computed from the GGA electronic structure are far too low. On the other hand, the self-consistent GGA + U^{ff} /cRPA scheme enables to find a unique self-consistent value of U^{ff} —within the range expected for a correct reproduction of experimental photoemission spectra—for some actinide dioxides (UO_2 , NpO_2), but underestimates the self-

consistent value for PuO_2 , and yields a too low value for AmO_2 and CmO_2 .

(2) The main origin of the underestimation of the self-consistent value of U^{ff} is the rr screening, on the contrary to lanthanide metals where it is rather the rf screening [36] (we also compared projected local orbital and maximally localized Wannier functions, and found that the effect on U^{ff} and J^{ff} is small). It thus directly questions the underlying electronic structure: AmO_2 and CmO_2 are described as metals when U^{ff} is applied on the f orbitals. We suggest that taking into account both spin orbit coupling and AFM ordering could have an effect on the band gap for the DFT + U^{ff} electronic structure, and possibly on the screening processes causing the limitations of the scheme.¹⁷ However, a much better description of the density of states could be made by including the interaction on oxygen p orbitals in DFT + U or by using hybrid functionals or GW which would lower the energy of the p bands, and hence, lower the screening in AmO_2 and CmO_2 . Such a better description could lead to larger values of U^{ff} , as suggested by the calculation of U^{ff} on the basis of self-consistent GW .

(3) Changing the model for correlated electrons and taking into account the interaction on oxygen p orbitals [35] solves the limitations of the self-consistent f model regardless of the electronic structure calculation method and regardless of the details of the electronic structure near the Fermi level. Since more states are included in the correlated subspace, the constrained screening decreases, so that the dependence of the cRPA value U_{out}^{ff} as a function of U_{in}^{ff} is lower, as we have shown; as a consequence, finding a well defined self-consistent value of U^{ff} should be easier.

This underlines the need of taking into account all interactions among both oxygen p and actinide f orbitals, since these interactions are important, and the need of taking into account correlation on oxygen p orbitals in the electronic structure, in order to describe correctly the screening of ff interaction by p electrons (as shown by GW calculations [23]). The drawback of the fp model for these systems would be the high computational cost of the solution of the many body model since the dimension of the correlated space would be larger unless a shell-folding scheme is used as proposed in Ref. [35].

ACKNOWLEDGMENTS

We thank Grégory Geneste and Martin S. Talla Noutack for useful discussions. The calculations were performed by using the supercomputers of the Commissariat à l'Énergie Atomique et aux Énergies Alternatives (CEA) at Bruyères-le-Châtel. We also thank the anonymous referees for their suggestions in order to improve the paper.

¹⁷In addition, enabling structural relaxation instead of merely fixing the cell parameter to its experimental value may increase the band gap—as shown for AmO_2 in Ref. [67]—and thus, modify furtherly the screening processes underlying the limitations of the scheme.

TABLE VI. Electronic structure of isolated actinide (An) atoms [72] (from uranium to curium), and number N_e of $5f$ electrons on each actinide atom inside the considered dioxide (AnO_2) crystal.

Actinide (An)	Electronic structure (isolated An atom)	N_e (AnO_2)
U	[Rn] $7s^2 5f^3 6d^1$	2
Np	[Rn] $7s^2 5f^4 6d^1$	3
Pu	[Rn] $7s^2 5f^6$	4
Am	[Rn] $7s^2 5f^7$	5
Cm	[Rn] $7s^2 5f^7 6d^1$	6

APPENDIX A: GGA + U^{ff} ELECTRONIC STRUCTURE: NUMBER OF f ELECTRONS AND OCCUPATION NUMBERS

1. Number of f electrons on actinide atoms

In this Appendix, we discuss the number of correlated electrons on actinide atoms inside the actinide dioxide crystal.

Electronic structure of isolated atoms of actinides from uranium to curium [72] is given in Table VI. Inside the corresponding actinide dioxides, four electrons from each actinide atom contribute to the bonding with oxygen atoms [73]. These electrons are taken first among $7s$ and $6d$ orbitals, then among $5f$ orbitals, so that the number N_e of $5f$ electrons remaining on each actinide atom inside the dioxide—also given in Table VI—is diminished. Thus, for DFT + U calculations, we initialize the occupation matrices with the corresponding number N_e of $5f$ electrons.

2. GGA + U^{ff} occupation numbers

In this Appendix, we comment the evolution of the number of electrons as a function of U^{ff} for actinide dioxides.

(1) For UO_2 , the number of correlated electrons ($N_e = 2$) is not compatible with cubic symmetry, which is already broken at low values of U : up to 6.0 eV, one electron is localized in a T_{1u} orbital, whereas the other is in a hybridized state between a T_{1u} orbital and a T_{2u} orbital. The latter configuration corresponds to the ground state found in the antiferromagnetic phase in Ref. [21], for $U^{ff} = 4.5$ eV and $J^{ff} = 0.51$ eV. From 7.0 eV, the T_{2u} orbitals become more favorable energetically. Because of the repulsion term in DFT + U^{ff} , the two electrons are localized in two T_{2u} orbitals rather than being shared between the three T_{2u} orbitals.

(2) For NpO_2 , the number of correlated electrons ($N_e = 3$) is compatible with cubic symmetry. The 3 electrons localize in the 3 T_{2u} orbitals.

(3) For PuO_2 , the number of correlated electrons ($N_e = 4$) is compatible with cubic symmetry, but, whereas three electrons are localized in the T_{2u} orbitals, the last one is localized in a T_{1u} orbital even at low (nonzero) values of U^{ff} , breaking the symmetry.

(4) For AmO_2 , the number of correlated electrons ($N_e = 5$) is not compatible with cubic symmetry. The latter is preserved up to $U^{ff} = 3.0$ eV; from $U^{ff} = 4.0$ eV, the electrons shared between the T_{1u} orbitals localize in two of the latter.

TABLE VII. Ground state occupations of CRSH orbitals (spin \uparrow), within GGA ($U^{ff} = J^{ff} = 0.0$ eV) and GGA + U^{ff} (for several values of U^{ff} and values of J^{ff} given in Table IV), for actinide dioxides from uranium to curium.

UO_2								
U (eV)	J (eV)	T_{1u}			A_{2u}	T_{2u}		
0.0	0.0	0.35	0.35	0.35	0.15	0.33	0.33	0.33
3.0	0.57	1	0.6	0	0	0	0.3	0
6.0	0.57	1	0.6	0	0	0	0.3	0
7.0	0.57	0	0	0	0	0	1	1
10.0	0.57	0	0	0	0	0	1	1
NpO_2								
U (eV)	J (eV)	T_{1u}			A_{2u}	T_{2u}		
0.0	0.0	0.43	0.43	0.43	0.16	0.57	0.57	0.57
2.0	0.6	0.07	0.07	0.07	0.10	0.93	0.93	0.93
10.0	0.6	0.02	0.02	0.02	0.05	0.96	0.96	0.96
PuO_2								
U (eV)	J (eV)	T_{1u}			A_{2u}	T_{2u}		
0.0	0.0	0.59	0.59	0.59	0.22	0.80	0.80	0.80
2.0	0.63	0.16	0.16	0.94	0.16	0.93	0.93	0.93
10.0	0.63	0.08	0.08	0.99	0.09	0.93	0.93	0.93
AmO_2								
U (eV)	J (eV)	T_{1u}			A_{2u}	T_{2u}		
0.0	0.0	0.76	0.76	0.76	0.35	0.90	0.90	0.90
2.0	0.67	0.75	0.75	0.75	0.22	0.94	0.94	0.94
3.0	0.67	0.77	0.77	0.77	0.19	0.95	0.95	0.95
4.0	0.67	0.35	0.92	0.92	0.19	0.96	0.96	0.96
10.0	0.67	0.06	0.97	0.97	0.14	0.97	0.97	0.97
CmO_2								
U (eV)	J (eV)	T_{1u}			A_{2u}	T_{2u}		
0.0	0.0	0.91	0.91	0.91	0.67	0.96	0.96	0.96
2.0	0.70	0.92	0.92	0.92	0.65	0.96	0.96	0.96
9.0	0.70	0.96	0.96	0.96	0.86	0.97	0.97	0.97

(5) For CmO_2 , the calculation is performed by considering $N_e = 6$ correlated electrons in the occupation matrices (which is compatible with cubic symmetry). During the calculation, the number of correlated electrons increases. Cubic symmetry is preserved regardless the value of U^{ff} . All T_{1u} and T_{2u} orbitals are filled, whereas the occupation of the A_{2u} orbital increases with U^{ff} , which we interpret as a consequence of hybridization between $5f$ states and $2p$ states from oxygen.

APPENDIX B: INFLUENCE OF THE LOCALIZATION OF CORRELATED ORBITALS ON CRPA EFFECTIVE INTERACTIONS IN UO_2 .

In this Appendix, we study the role of the localization of correlated orbitals on the value of effective interactions by using two types of correlated orbitals, namely, the PLO Wannier functions and ML Wannier functions. We do this comparison for uranium dioxide only.

Starting from the GGA electronic structure of nonmagnetic UO_2 (the corresponding density of states is shown in upper

TABLE VIII. Values of direct and exchange bare interactions ($U_{\text{bare}}, J_{\text{bare}}$), and direct and exchange cRPA interactions ($U_{\text{cRPA}}, J_{\text{cRPA}}$) (in eV), for UO_2 in nonmagnetic GGA, for each model considered, for projected local orbital (PLOWF) and maximally localized (MLWF) Wannier functions. We remind [33,44] that (a) and (b) refer to the way the polarization is computed. In (a), transitions inside selected bands are excluded from the polarizability calculation. Whereas for (b), we use the weighting factor detailed in Refs. [33,43,44].

Model	$f-f$	$f-fp$ (a)	$f-fp$ (b)	$fp-fp$
PLOWF				
U_{bare} (eV)	15.52	16.47	16.47	16.47
J_{bare} (eV)	0.58	0.66	0.66	0.66
U_{cRPA} (eV)	3.43	3.63	2.03	6.18
J_{cRPA} (eV)	0.47	0.54	0.53	0.55
MLWF				
U_{bare} (eV)	16.03	17.07	17.07	17.07
J_{bare} (eV)	0.61	0.69	0.69	0.69
U_{cRPA} (eV)	3.54	3.76	2.21	6.42
J_{cRPA} (eV)	0.49	0.56	0.55	0.57

panel of Fig. 1), we compute bare and effective (both direct and exchange) interactions within cRPA, for the $f-f$, $f-fp$, and $fp-fp$ models presented in Sec. II B. Results are given in Table VIII.

1. Comparison of the different models

We briefly comment the variation of the values according to the model. These calculations were already discussed in, e.g., Refs. [33,35].

The bare interaction increases for the $f-fp$ and $fp-fp$ models with respect to the $f-f$ model. This is because more Kohn-Sham wave functions are used for the construction of Wannier functions, which increases their localization and, thus, the bare interaction. The cRPA values are larger in $f-fp$ (a) case with respect to the $f-f$ case for the same reason since, in this case, the screening is the same. In $f-fp$ (b), the screening is larger, because there are remaining transitions near the Fermi level, due to the use of the weighting coefficient scheme, so that U^{ff} is smaller (see Ref. [33]). Lastly, the $fp-fp$ (a) model yields a high value of U , since the screening is weaker than for all other models.

2. Comparison of PLO and ML Wannier functions

We observe that all values increase slightly in the case of ML Wannier functions with respect to the case of PLO Wannier functions ($\simeq 0.5\text{--}0.6$ eV for U_{bare} , $\simeq 0.1\text{--}0.3$ eV for U_{out}), which is a consequence of the increased localisation with respect to the PLO Wannier functions. This shows that the use of ML Wannier functions only brings a small quantitative correction to the use of PLO Wannier functions.

- [1] Y. Baer and J. Schoenes, Electronic structure and coulomb correlation energy in UO_2 single crystal, *Solid State Commun.* **33**, 885 (1980).
- [2] T. M. McCleskey, E. Bauer, Q. Jia, A. K. Burrell, B. L. Scott, S. D. Conradson, A. Mueller, L. Roy, X. Wen, G. E. Scuseria, and R. L. Martin, Optical band gap of NpO_2 and PuO_2 from optical absorbance of epitaxial films, *J. Appl. Phys.* **113**, 013515 (2013).
- [3] B. W. Veal, D. J. Lam, H. Diamond, and H. R. Hoekstra, X-ray photoelectron-spectroscopy study of oxides of the transuranium elements Np, Pu, Am, Cm, Bk, and Cf, *Phys. Rev. B* **15**, 2929 (1977).
- [4] K. T. Moore and G. van der Laan, Nature of the $5f$ states in actinide metals, *Rev. Mod. Phys.* **81**, 235 (2009).
- [5] A. Kotani and T. Yamazaki, Systematic analysis of core photoemission spectra for actinide di-oxides and rare-earth sesqui-oxides, *Prog. Theor. Phys. Suppl.* **108**, 117 (1992).
- [6] L. E. Roy, T. Durakiewicz, R. L. Martin, J. E. Peralta, G. E. Scuseria, C. G. Olson, J. J. Joyce, and E. Guzewicz, Dispersion in the mott insulator UO_2 : A comparison of photoemission spectroscopy and screened hybrid density functional theory, *J. Comput. Chem.* **29**, 2288 (2008).
- [7] P. Hohenberg and W. Kohn, Inhomogeneous electron gas, *Phys. Rev.* **136**, B864 (1964).
- [8] W. Kohn and L. J. Sham, Self-consistent equations including exchange and correlation effects, *Phys. Rev.* **140**, A1133 (1965).
- [9] D. C. Langreth and J. P. Perdew, Theory of nonuniform electronic systems. I. Analysis of the gradient approximation and a generalization that works, *Phys. Rev. B* **21**, 5469 (1980).
- [10] J. P. Perdew and A. Zunger, Self-interaction correction to density-functional approximations for many-electron systems, *Phys. Rev. B* **23**, 5048 (1981).
- [11] J. Heyd and G. E. Scuseria, Efficient hybrid density functional calculations in solids: Assessment of the Heyd–Scuseria–Ernzerhof screened coulomb hybrid functional, *J. Chem. Phys.* **121**, 1187 (2004).
- [12] L. Petit, A. Svane, Z. Szotek, W. M. Temmerman, and G. M. Stocks, Electronic structure and ionicity of actinide oxides from first principles, *Phys. Rev. B* **81**, 045108 (2010).
- [13] I. D. Prodan, G. E. Scuseria, and R. L. Martin, Assessment of metageneralized gradient approximation and screened coulomb hybrid density functionals on bulk actinide oxides, *Phys. Rev. B* **73**, 045104 (2006).
- [14] I. D. Prodan, G. E. Scuseria, and R. L. Martin, Covalency in the actinide dioxides: Systematic study of the electronic properties using screened hybrid density functional theory, *Phys. Rev. B* **76**, 033101 (2007).
- [15] X.-D. Wen, R. L. Martin, L. E. Roy, G. E. Scuseria, S. P. Rudin, E. R. Batista, T. M. McCleskey, B. L. Scott, E. Bauer, J. J. Joyce, and T. Durakiewicz, Effect of spin-orbit coupling on the actinide dioxides AnO_2 ($\text{An}=\text{Th}, \text{Pa}, \text{U}, \text{Np}, \text{Pu}, \text{and Am}$): A screened hybrid density functional study, *J. Chem. Phys.* **137**, 154707 (2012).

- [16] V. I. Anisimov and O. Gunnarsson, Density-functional calculation of effective coulomb interactions in metals, *Phys. Rev. B* **43**, 7570 (1991).
- [17] A. Georges and G. Kotliar, Hubbard model in infinite dimensions, *Phys. Rev. B* **45**, 6479 (1992).
- [18] A. Georges, G. Kotliar, W. Krauth, and M. J. Rozenberg, Dynamical mean-field theory of strongly correlated fermion systems and the limit of infinite dimensions, *Rev. Mod. Phys.* **68**, 13 (1996).
- [19] V. I. Anisimov, A. I. Poteryaev, M. A. Korotin, A. O. Anokhin, and G. Kotliar, First-principles calculations of the electronic structure and spectra of strongly correlated systems: Dynamical mean-field theory, *J. Phys.: Condens. Matter* **9**, 7359 (1997).
- [20] M. C. Gutzwiller, Effect of Correlation on the Ferromagnetism of Transition Metals, *Phys. Rev. Lett.* **10**, 159 (1963).
- [21] B. Dorado, B. Amadon, M. Freyss, and M. Bertolus, DFT + U calculations of the ground state and metastable states of uranium dioxide, *Phys. Rev. B* **79**, 235125 (2009).
- [22] B.-T. Wang, H. Shi, W. Li, and P. Zhang, First-principles LDA + u and GGA + u study of neptunium dioxide, *Phys. Rev. B* **81**, 045119 (2010).
- [23] Q. Yin, A. Kutepov, K. Haule, G. Kotliar, S. Y. Savrasov, and W. E. Pickett, Electronic correlation and transport properties of nuclear fuel materials, *Phys. Rev. B* **84**, 195111 (2011).
- [24] G. Jomard, B. Amadon, F. Bottin, and M. Torrent, Structural, thermodynamic, and electronic properties of plutonium oxides from first principles, *Phys. Rev. B* **78**, 075125 (2008).
- [25] Y. Lu, Y. Yang, F. Zheng, B.-T. Wang, and P. Zhang, Electronic, mechanical, and thermodynamic properties of americium dioxide, *J. Nucl. Mater.* **441**, 411 (2013).
- [26] J. c. v. Kolorenč, A. B. Shick, and A. I. Lichtenstein, Electronic structure and core-level spectra of light actinide dioxides in the dynamical mean-field theory, *Phys. Rev. B* **92**, 085125 (2015).
- [27] L. Huang, Y. Wang, and P. Werner, Pressure-driven insulator-metal transition in cubic phase UO₂, *Europhys. Lett.* **119**, 57007 (2017).
- [28] L. Hou, W.-D. Li, F. Wang, O. Eriksson, and B.-T. Wang, Structural, electronic, and thermodynamic properties of curium dioxide: Density functional theory calculations, *Phys. Rev. B* **96**, 235137 (2017).
- [29] B. Amadon, First-principles DFT + DMFT calculations of structural properties of actinides: Role of Hund's exchange, spin-orbit coupling, and crystal structure, *Phys. Rev. B* **94**, 115148 (2016).
- [30] R. Qiu, B. Ao, and L. Huang, Effective coulomb interaction in actinides from linear response approach, *Comput. Mater. Sci.* **171**, 109270 (2020).
- [31] F. Aryasetiawan, M. Imada, A. Georges, G. Kotliar, S. Biermann, and A. I. Lichtenstein, Frequency-dependent local interactions and low-energy effective models from electronic structure calculations, *Phys. Rev. B* **70**, 195104 (2004).
- [32] F. Aryasetiawan, K. Karlsson, O. Jepsen, and U. Schönberger, Calculations of hubbard u from first-principles, *Phys. Rev. B* **74**, 125106 (2006).
- [33] B. Amadon, T. Applencourt, and F. Bruneval, Screened coulomb interaction calculations: cRPA implementation and applications to dynamical screening and self-consistency in uranium dioxide and cerium, *Phys. Rev. B* **89**, 125110 (2014).
- [34] B. Amadon, T. Applencourt, and F. Bruneval, Erratum: Screened coulomb interaction calculations: cRPA implementation and applications to dynamical screening and self-consistency in uranium dioxide and cerium [Phys. Rev. B 89, 125110 (2014)], *Phys. Rev. B* **96**, 199907(E) (2017).
- [35] P. Seth, P. Hansmann, A. van Roekeghem, L. Vaugier, and S. Biermann, Towards a First-Principles Determination of Effective Coulomb Interactions in Correlated Electron Materials: Role of Intershell Interactions, *Phys. Rev. Lett.* **119**, 056401 (2017).
- [36] J.-B. Morée and B. Amadon, First-principles calculation of coulomb interaction parameters for lanthanides: Role of self-consistency and screening processes, *Phys. Rev. B* **98**, 205101 (2018).
- [37] K. Karlsson, F. Aryasetiawan, and O. Jepsen, Method for calculating the electronic structure of correlated materials from a truly first-principles LDA + u scheme, *Phys. Rev. B* **81**, 245113 (2010).
- [38] N. Marzari and D. Vanderbilt, Maximally localized generalized wannier functions for composite energy bands, *Phys. Rev. B* **56**, 12847 (1997).
- [39] I. Souza, N. Marzari, and D. Vanderbilt, Maximally localized wannier functions for entangled energy bands, *Phys. Rev. B* **65**, 035109 (2001).
- [40] N. Marzari, A. A. Mostofi, J. R. Yates, I. Souza, and D. Vanderbilt, Maximally localized wannier functions: Theory and applications, *Rev. Mod. Phys.* **84**, 1419 (2012).
- [41] A. A. Mostofi, J. R. Yates, G. Pizzi, Y.-S. Lee, I. Souza, D. Vanderbilt, and N. Marzari, An updated version of WANNIER90: A tool for obtaining maximally-localised wannier functions, *Comput. Phys. Commun.* **185**, 2309 (2014).
- [42] B. Amadon, F. Lechermann, A. Georges, F. Jollet, T. O. Wehling, and A. I. Lichtenstein, Plane-wave based electronic structure calculations for correlated materials using dynamical mean-field theory and projected local orbitals, *Phys. Rev. B* **77**, 205112 (2008).
- [43] B.-C. Shih, Y. Zhang, W. Zhang, and P. Zhang, Screened coulomb interaction of localized electrons in solids from first principles, *Phys. Rev. B* **85**, 045132 (2012).
- [44] R. Sakuma and F. Aryasetiawan, First-principles calculations of dynamical screened interactions for the transition metal oxides Mo ($M = Mn, Fe, Co, Ni$), *Phys. Rev. B* **87**, 165118 (2013).
- [45] M. Cococcioni and S. de Gironcoli, Linear response approach to the calculation of the effective interaction parameters in the LDA + U method, *Phys. Rev. B* **71**, 035105 (2005).
- [46] S.-G. Park, B. Magyari-Köpe, and Y. Nishi, Electronic correlation effects in reduced rutile TiO₂ within the LDA + u method, *Phys. Rev. B* **82**, 115109 (2010).
- [47] L. A. Agapito, S. Curtarolo, and M. Buongiorno Nardelli, Reformulation of DFT + u as a Pseudohybrid Hubbard Density Functional for Accelerated Materials Discovery, *Phys. Rev. X* **5**, 011006 (2015).
- [48] B. Amadon, F. Jollet, and M. Torrent, γ and β cerium: LDA + u calculations of ground-state parameters, *Phys. Rev. B* **77**, 155104 (2008).
- [49] G. Geneste, B. Amadon, M. Torrent, and G. Dezanneau, DFT + u study of self-trapping, trapping, and mobility of oxygen-type hole polarons in barium stannate, *Phys. Rev. B* **96**, 134123 (2017).

- [50] U. Benedict and W. Holzapfel, Chapter 113 high-pressure studies – structural aspects, in *Lanthanides/Actinides: Physics I*, Handbook on the Physics and Chemistry of Rare Earths, Vol. 17 (Elsevier, Amsterdam, 1993), pp. 245–300.
- [51] V. Sobolev, Thermophysical properties of NpO_2 , AmO_2 and CmO_2 , *J. Nucl. Mater.* **389**, 45 (2009), thermochemistry and Thermophysics of Nuclear Materials.
- [52] L. Petit, A. Svane, Z. Szotek, and W. M. Temmerman, First-principles calculations of $\text{PuO}_2 \pm x$, *Science* **301**, 498 (2003).
- [53] W. Jones, J. Gordon, and E. Long, The heat capacities of uranium, uranium trioxide, and uranium dioxide from 15 k to 300 k, *J. Chem. Phys.* **20**, 695 (1952).
- [54] J. Ross and D. Lam, The magnetic susceptibility of neptunium oxide and carbide between 4.2 and 350 k, *J. Appl. Phys.* **38**, 1451 (1967).
- [55] G. Raphael and R. Lallement, Susceptibilite magnetique de PuO_2 , *Solid State Commun.* **6**, 383 (1968).
- [56] D. Karraker, Magnetic susceptibility of 243AmO_2 , *J. Chem. Phys.* **63**, 3174 (1975).
- [57] S. E. Nave, R. G. Haire, and P. G. Huray, Magnetic properties of actinide elements having the $5f6$ and $5f7$ electronic configurations, *Phys. Rev. B* **28**, 2317 (1983).
- [58] A. Arrott and J. E. Goldman, Magnetic susceptibility of UO_2 from 2-degrees-k to 300-degrees-k, *Phys. Rev.* **99**, 1641 (1955).
- [59] D. Cox and B. Frazer, A neutron diffraction study of NpO_2 , *J. Phys. Chem. Solids* **28**, 1649 (1967).
- [60] P. E. Blöchl, Projector augmented-wave method, *Phys. Rev. B* **50**, 17953 (1994).
- [61] M. Torrent, F. Jollet, F. Bottin, G. Zerah, and X. Gonze, Implementation of the projector augmented-wave method in the abinit code: Application to the study of iron under pressure, *Comput. Mater. Sci.* **42**, 337 (2008).
- [62] B.-T. Wang, P. Zhang, R. Lizárraga, I. Di Marco, and O. Eriksson, Phonon spectrum, thermodynamic properties, and pressure-temperature phase diagram of uranium dioxide, *Phys. Rev. B* **88**, 104107 (2013).
- [63] P. Zhang, B.-T. Wang, and X.-G. Zhao, Ground-state properties and high-pressure behavior of plutonium dioxide: Density functional theory calculations, *Phys. Rev. B* **82**, 144110 (2010).
- [64] P. Larson, W. R. L. Lambrecht, A. Chantis, and M. van Schilfhaarde, Electronic structure of rare-earth nitrides using the LSDA + u approach: Importance of allowing $4f$ orbitals to break the cubic crystal symmetry, *Phys. Rev. B* **75**, 045114 (2007).
- [65] J. Schoenes, Optical properties and electronic structure of UO_2 , *J. Appl. Phys.* **49**, 1463 (1978).
- [66] C. Suzuki, T. Nishi, M. Nakada, M. Akabori, M. Hirata, and Y. Kaji, Core-hole effect on xanes and electronic structure of minor actinide dioxides with fluorite structure, *J. Phys. Chem. Solids* **73**, 209 (2012).
- [67] M. S. Talla Noutack, G. Geneste, G. Jomard, and M. Freyss, First-principles investigation of the bulk properties of americium dioxide and sesquioxides, *Phys. Rev. Materials* **3**, 035001 (2019).
- [68] X.-D. Wen, R. Martin, T. M. Henderson, and G. E. Scuseria, Density functional theory studies of the electronic structure of solid state actinide oxides, *Chem. Rev.* **113**, 1063 (2013).
- [69] Q. Han, B. Chakrabarti, and K. Haule, Investigation into the inadequacy of cRPA in reproducing screening in strongly correlated systems, (2018).
- [70] D. Van Der Marel, The Electronic Structure of Embedded Transition Metal Atoms, Ph.D. thesis, 1985.
- [71] H. Jiang, Revisiting the gw approach to d - and f -electron oxides, *Phys. Rev. B* **97**, 245132 (2018).
- [72] G. L. Miessler and D. A. Tarr, *Inorganic Chemistry*, 2nd ed. (Prentice-Hall, Northfield, Minnesota, 1999), p. 38.
- [73] N. S. Christiane Bonnelle, *Rare-Earths and Actinides in High Energy Spectroscopy* (Springer Netherlands, 2015).